

Direct Synthesis of Copper and Copper Oxide Nanoparticles from Bulk Materials by the Induction Flow Levitation Technique

A. A. Kapinos^a, A. N. Markov^a, A. N. Petukhov^a,
K. V. Otvagina^a, O. V. Kazarina^a, and A. V. Vorotyntsev^{a, *}

^a Lobachevsky State University, Nizhny Novgorod, 603022 Russia

*e-mail: an.vorotyntsev@gmail.com

Received March 12, 2022; revised May 19, 2022; accepted June 14, 2022

Abstract—Cu, Cu@Cu₂O, and CuO nanoparticles have been prepared by the induction flow levitation method using bulk copper. The method offers a number of advantages, such as a high production rate, continuity of the nanoparticle synthesis process, the ability to vary the nanoparticle size in a wide range, and contactless heating, which ensures high purity of the synthesis product. To obtain nanoparticles with a core–shell structure and copper oxide nanoparticles, oxygen was introduced into different zones of the quartz reactor used. The synthesized nanoparticles have been characterized by a number of physicochemical methods.

Keywords: copper, nanoparticles, core–shell, induction flow levitation

DOI: 10.1134/S0020168522090060

INTRODUCTION

Nanoparticle-based materials have novel, unique properties compared to bulk materials owing to the large ratio of their specific surface area to their volume [1, 2]. Metallic nanoparticles have found application as catalysts [3], in biosensors [4], for information storage [5], in optics [6], and in medicine for diagnosis and treatment of diseases [7, 8].

For example, the high catalytic activity of copper nanoparticles has aroused increased attention for application in organic syntheses [9, 10]. Photocatalytic properties of copper are employed for removing organic dyes from wastewater on an industrial scale [11]. Owing to their rather high electrical conductivity, copper nanoparticles are used in conductive ink and electronics [12, 13]. In addition, copper nanoparticles have antibacterial and antimicrobial properties [14–16].

The main drawback to copper nanoparticles, limiting their use, is their susceptibility to oxidation and, as a consequence, strong aggregation during storage [17]. One way to resolve this problem is to prepare nanoparticles with a core–shell structure [18].

Cu@Cu₂O nanoparticles can be used in photocatalytic conversion of CO₂ into HCOOH [19]. In addition, such nanoparticles were shown to exhibit catalytic activity for hydrogen generation from ammonia borane via hydrolysis [20, 21].

In the past few years, nanoparticles have been synthesized by a variety of techniques, which can be divided into physical and chemical ones. The physical techniques include pulsed laser ablation [22], plane-

tary ball milling [23], physical vapor deposition [24], and others. The chemical synthesis techniques include sol–gel processing [25], chemical reduction [26], sonochemical synthesis [27], electrochemical deposition [28], hydrothermal treatment [13], and others. The use of dangerous chemical substances, high temperatures, and complex implementation limit industrial applications of these techniques.

At present, one of the most promising ways of preparing nanoparticles is induction flow levitation (IFL). Its main advantages are high production rate (up to 100 g/h), the ability to tailor the nanoparticle size in a wide range (0.5–500 nm), contactless heating (up to 2500°C), and the absence of harmful by-products, which ensures high purity of the nanoparticles produced by and environmental friendliness of this technique. A distinctive feature of this technique is evaporation of a levitating metal in the high-frequency field of a specially designed inductor. Even though the IFL (Gen–Miller) technique was discovered in the early 1960s, it has not found wide application in industry. At present, more and more research groups are studying the capabilities of this technique for the preparation of nanoparticles of metals and their compounds. In a previous report, Markov et al. [29] described the preparation of titanium nanoparticles by the IFL technique in flowing argon, and the addition of hydrogen as a reaction gas allowed Kuskov et al. [30] to obtain titanium hydride nanoparticles.

The purpose of this work was to prepare Cu, Cu@Cu₂O, and CuO nanoparticles with an average size under 40 nm by the IFL technique in flowing

argon. To obtain Cu@Cu₂O and CuO nanoparticles, oxygen was added to the carrier gas flow in different zones of a quartz reactor, which led to the formation of different types of copper-containing nanoparticles.

EXPERIMENTAL

Materials. The starting materials used were 0.5-mm-diameter copper wire (99.999% purity, Sigma-Aldrich, Germany), extrapure-grade hexane (OOO Komponent-reaktiv, Russia); argon (99.9995%, OOO Monitoring, Russia), and oxygen (99.9995%, OOO Monitoring, Russia).

Experimental setup and synthesis procedure. Figure 1 shows a schematic of our experimental setup. A bulk sample was suspended on a feed wire in a quartz reactor and had the form of a small wire ball weighing 0.5 g. In the first step, the system was pumped down to a vacuum of 10⁻³ to 10⁻² mbar over a period of 3 h in order to remove the trace levels of water and air present (the pressure was monitored with a Pfeifer Vacuum sensor (United States)). In the second step, the system was filled with an inert gas to atmospheric pressure and a coolant gas was introduced at a flow rate of 10 L/min (the flow rate was controlled by a Bronkhorst gas mass flow controller (Netherlands)). A voltage was applied to the inductor, resulting in induction heating of the sample, which melted while levitating. For a droplet of the molten metal to levitate, the inductor, made of a 3-mm-diameter copper tube, had three lower and two upper counter-wound turns (Fig. 2a). Heating to a temperature above the melting point of copper caused vaporization of atoms from the surface of the molten metal. In this process, a dense flow of forming nanoparticles could be visually observed (Fig. 2b).

To feed the sample being evaporated, immediately after the beginning of vaporization of atoms the droplet was replenished by continuously feeding 0.5-mm-diameter wire to the molten droplet. This small wire diameter was chosen in order to minimize the effect of the temperature gradient on the levitating sample. Besides, wire of this diameter is “invisible” to an electromagnetic field. Starting at this instant, “process stabilization” began, which took 60 min. This step was needed to reach steady-state synthesis conditions. Vaporizing metal atoms were detached by the carrier gas flow from the droplet surface, forming nanoparticles in the condensation zone, which were then collected on filter 1. After 60 min, we turned off the valve to filter 1 and turned on the valve to filter 2, where the nanoparticles were collected for subsequent characterization (operating time, 60–120 min). Filter 2 was equipped with an electromagnetic shaker, which was automatically turned on if the pressure in the system increased by 0.01 mbar. The increase in pressure in the system was caused by filter clogging with nanoparticles. To ascertain that the process was steady-state, the temperature of the levitating sample was monitored

with an IMPAC ISR 6 infrared pyrometer (Advanced Energy Industries Inc., United States). The nanoparticle synthesis process was stopped by switching the carrier gas flow with nanoparticles back to filter 1, and the valves located before and after filter 2 were turned off in order to keep the synthesized nanoparticles in the inert (argon) atmosphere. Next, the voltage applied to the inductor was reduced to the lowest level at which the molten sample levitated in order to lower its temperature and terminate vaporization of atoms from its surface. In the final step, the voltage was switched off, and the droplet dropped (due to gravity) to a specialty collector in the form of a boron nitride beaker in the lower part of the apparatus.

To prepare Cu@Cu₂O nanoparticles, we used a reactor with an additional side inlet for introducing oxygen at a flow rate of 3 L/min into the condensation zone through a specially designed annular gap. Copper oxide nanoparticles were prepared by introducing oxygen together with argon from above into a direct-flow quartz reactor at flow rates of 3 and 10 L/min, respectively. In the first two cases, the pressure in the reactor was maintained at the level of atmospheric pressure, whereas to obtain copper oxide nanoparticles as small as possible the pressure in the system was maintained at a level of 400 mbar.

Subsequently, the synthesized copper nanoparticles were handled in an inert box (Mbraun Labstar, Germany) in an argon atmosphere containing less than 0.5 ppm of oxygen. Such handling was not needed in the case of Cu@Cu₂O or CuO nanoparticles because they were nonreactive with atmosphere oxygen.

For induction heating, we used a 10-kW high-frequency generator operating at a frequency of 0.44 MHz. The wire feed rate was 3 g/h.

Characterization techniques. The morphology of the Cu and Cu@Cu₂O nanoparticles was examined by transmission electron microscopy (TEM). Structural characteristics of the nanopowders were assessed by low-temperature (77 K) nitrogen adsorption measurements using BET analysis and the statistical thickness surface area (STSA) method. The phase composition of the samples was determined by X-ray diffraction. Using dynamic light scattering (DLS), TEM, BET, and X-ray diffraction data, we analyzed the nanoparticle size distribution and compared results obtained by different methods.

TEM and selected area electron diffraction (SAED). TEM and SAED data were obtained on a Carl Zeiss LIBRA 200 MC instrument (Germany) equipped with a Schottky field emission gun operating at 200 kV (resolving power of 0.12 nm). Samples were placed on standard TEM copper grids with a 200-mesh Lacey formvar supporting grid. The samples were prepared by ultrasonication of the nanoparticles in *n*-hexane, followed by deposition (“fishing”) on TEM grids.

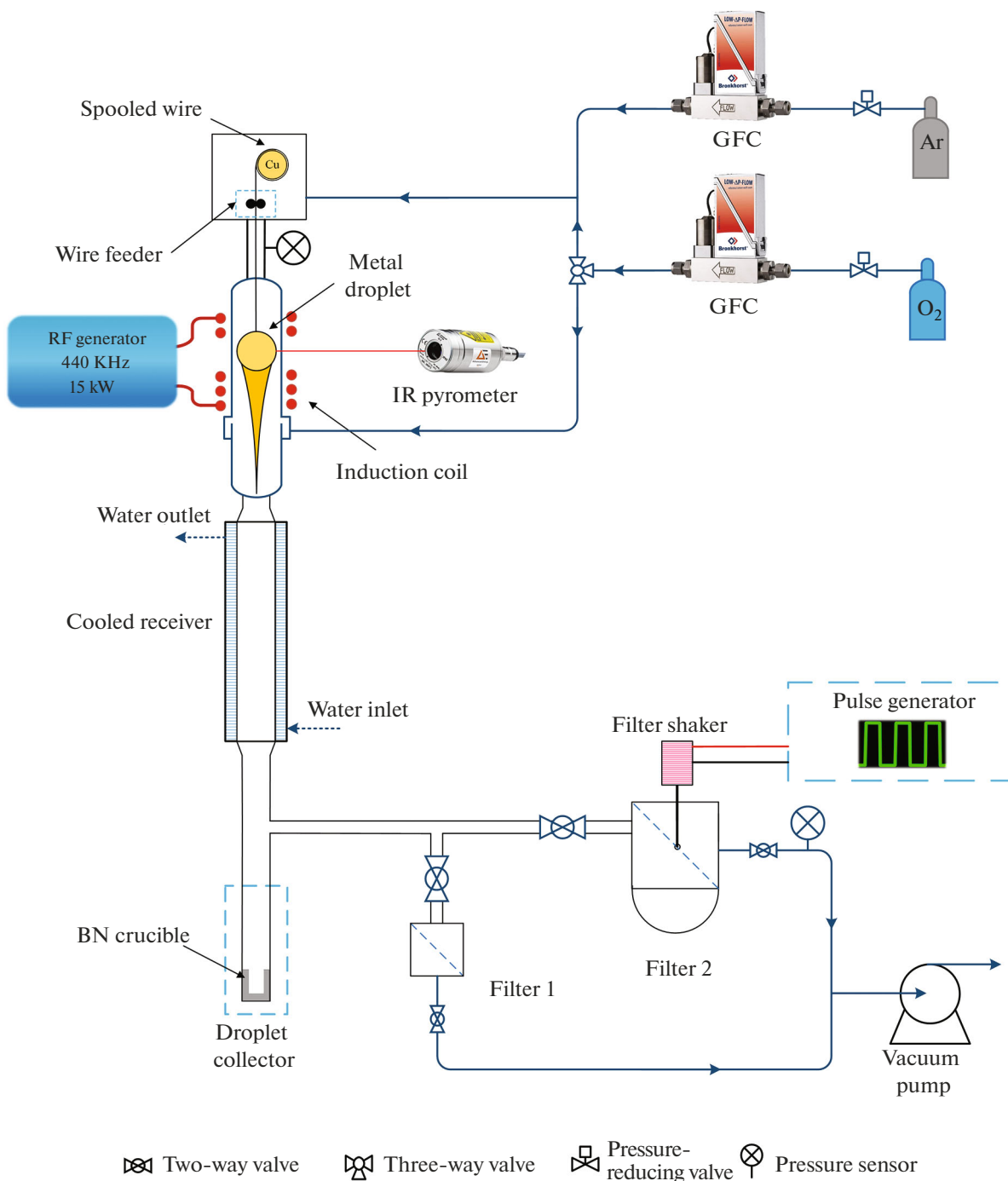


Fig. 1. Schematic of the experimental setup for the preparation of nanoparticles.

X-ray diffraction. The phase composition of the synthesized nanoparticles was determined by X-ray diffraction (Shimadzu XRD-7000 diffractometer, Japan). The measurements were performed at 40 kV and 30 mA. The width of the scatter slit in front of the detector was 0.3 mm. Intensity data were collected in the angular range $2\theta = 10^\circ\text{--}80^\circ$ with a scan step of 0.02° and counting time of 0.5 s per data point.

DLS. The nanoparticle size distribution was obtained using DLS on a NANO-flex II instrument (Microtrac Inc., United States), which made it possible to analyze particles 0.3 nm to 10 μm in size. The liquid phase used to prepare nanoparticle suspensions was *n*-hexane, with a zeta potential from 40 to 46 mV as determined using a NANO-flex Stabino instrument (Microtrac Inc., United States). The concentration of

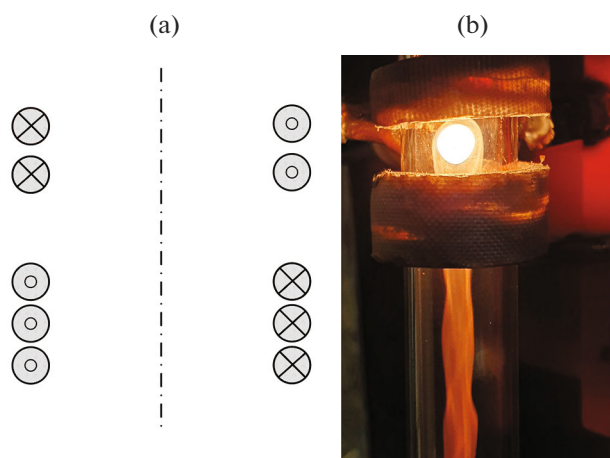


Fig. 2. (a) Schematic of the inductor and (b) observed flow of forming nanoparticles.

the suspensions was 1000 ppm. To disperse the nanoparticles, the suspensions were placed in an ultrasonic bath for 20 min.

Low-temperature nitrogen adsorption. The specific surface area and average particle size were evaluated from 77-K nitrogen adsorption/desorption isotherms obtained using SorbiMS instrument (OOO META, Russia). The surface area was determined by the BET and STSA methods. From the BET surface area, we evaluated the average particle size.

RESULTS AND DISCUSSION

As mentioned above, the IFL method is used to synthesize metal nanoparticles. At the same time, the use of oxidizing gases allows one to obtain metal oxide nanoparticles and core-shell nanoparticles possessing properties of metals, but having a protective crystalline layer up to 5 nm in thickness, which prevents further oxidation of the metal.

In our experiments, we chose reactor configurations that allowed us to obtain copper and copper oxide (CuO) nanoparticles in a flow reactor and core-shell nanoparticles in a reactor with a side inlet. The specific features of the reactor with a side inlet made it possible to obtain core-shell structures through the oxidation of a surface layer immediately after nanoparticle crystallization. Oxygen concentration was found to have a direct effect on the thickness of the oxide film on the synthesized nanostructures.

The morphology of the nanoparticles was examined by TEM. Figure 3a is a micrograph of copper nanoparticles in the form of agglomerates of spherical particles having an average diameter of 36 nm and a lognormal size distribution. The SAED pattern presented in Fig. 3b shows 111, 200, 220, 400, 311, 420, and 422 diffraction rings characteristic of copper.

The micrograph in Fig. 3c suggests that, introducing oxygen into the condensation zone through a specially designed annular gap, we obtained core-shell nanoparticles with an average size of 21 nm and average Cu₂O shell thickness of 2 nm. Figure 3d shows a SAED pattern of Cu@Cu₂O nanoparticles, which contains not only diffraction rings of copper, but also 200, 220, and 311 diffraction rings of Cu₂O. This indicates that the shell on the nanoparticle surface consists of the copper oxide Cu₂O.

The composition of the shell is due to the fact that oxygen was introduced through the annular ring into a laminar argon flow, so the oxygen distribution over the reaction zone (where the surface of the copper nanoparticles was oxidized) was nonuniform (the oxygen concentration increased with decreasing distance to the reactor wall). Since the flow of nanoparticles passed through the central part of the reactor, where oxygen concentration was lowest, the surface oxidation of the copper nanoparticles yielded copper(I) oxide.

Introducing an argon + oxygen mixture through the top part of the apparatus at a reduced pressure (400 mbar), we obtained CuO nanoparticles (Fig. 3d) in the form of isolated spheres with an average size of 5 nm. The SAED pattern in Fig. 3f shows 110, $\bar{1}11$, 111, $\bar{2}02$, 020, 202, $\bar{1}13$, 022, and 220 diffraction rings of copper(II) oxide.

Figure 4 shows the X-ray diffraction pattern of the copper nanoparticles prepared by the IFL method. We observed characteristic diffraction peaks of copper (PDF card no. 04-0836) located at $2\theta = 43.3^\circ$, 50.4° , and 74.1° and corresponding to the 111, 200, and 220 reflections from an FCC structure.

The X-ray diffraction pattern of the Cu@Cu₂O nanoparticles prepared after the addition of oxygen (Fig. 5) shows characteristic diffraction peaks of copper (Fig. 4) and the 111, 200, 220, and 311 reflections from copper(I) oxide, located at 36.4° , 42.3° , 61.3° , and 73.5° . The peak positions correspond to a Cu₂O standard (PDF card no. 05-0667).

The X-ray diffraction pattern of the CuO nanoparticles in Fig. 6 contains characteristic peaks of copper(II) oxide at $2\theta = 32.52^\circ$, 35.55° , 38.73° , 48.75° , 53.4° , 58.31° , 61.57° , 65.8° , and 68.13° (PDF card no. 48-1548): 110, $\bar{1}11$, 111, $\bar{2}02$, 020, 202, $\bar{1}13$, $\bar{3}11$, and 220.

It is worth noting that in none of the X-ray diffraction patterns of the three samples did we detect reflections from any impurity components. This indicates that the IFL method allows one to obtain high-purity nanoparticles. This is due, first, to contactless heating of the metal, preventing reaction of the molten droplet with parts of the experimental setup and, second, to the single-step nature of the method and the absence of additional contamination from the reagents used.

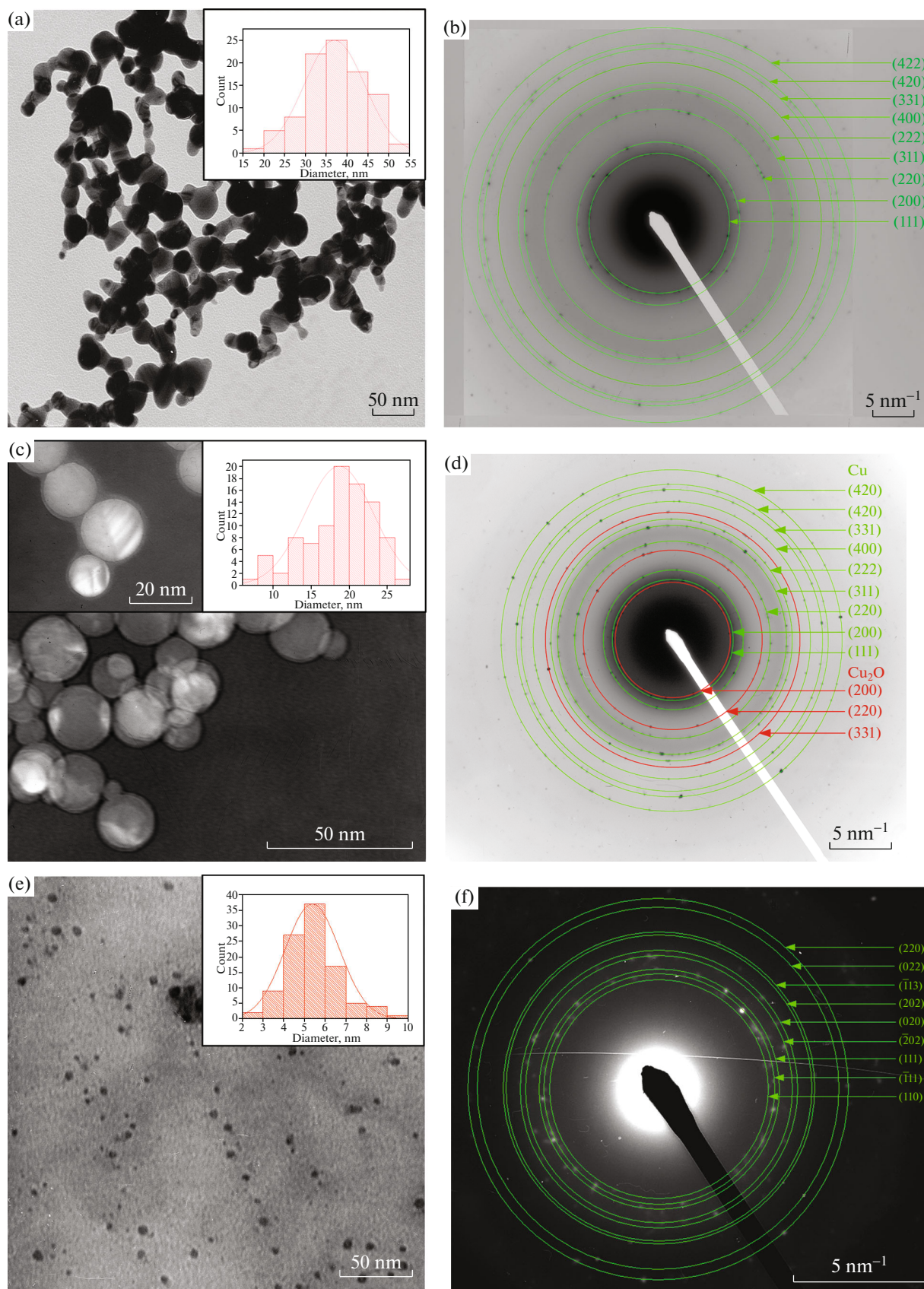


Fig. 3. (a, c, e) TEM images, size distributions, and (b, d, f) SAED patterns of (a, b) Cu, (c, d) Cu@Cu₂O, and (e, f) CuO nanoparticles.

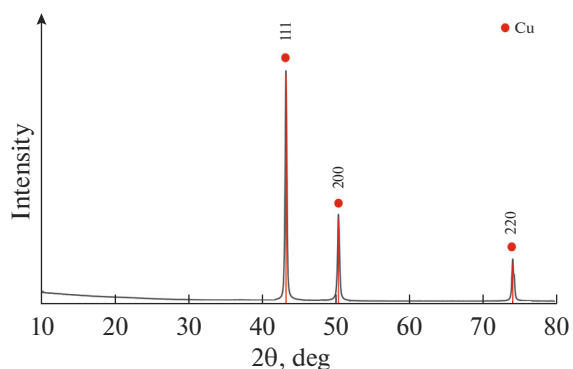


Fig. 4. X-ray diffraction pattern of the copper nanoparticles.

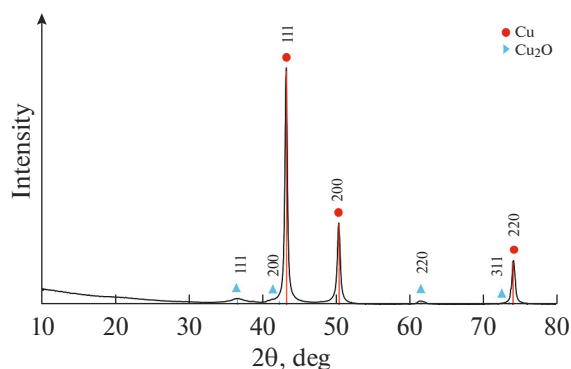


Fig. 5. X-ray diffraction pattern of the Cu@Cu₂O nanoparticles.

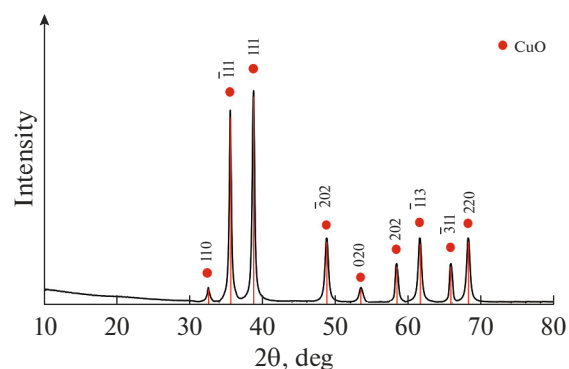


Fig. 6. X-ray diffraction pattern of the CuO nanoparticles.

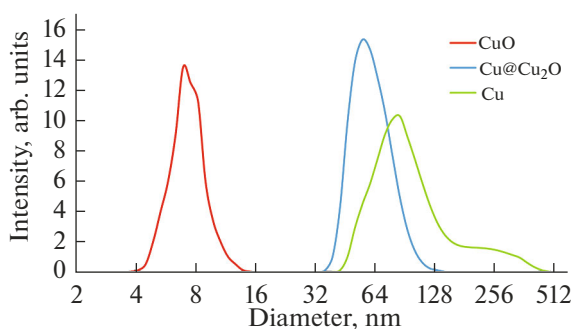


Fig. 7. Nanoparticle size distributions inferred from DLS data.

Using the X-ray diffraction patterns and Scherrer formula, we evaluated the average crystallite size (Table 1):

$$D = \frac{K\lambda}{\beta \cos\theta}, \quad (1)$$

where K is the Scherrer constant ($K = 0.94$), λ is the X-ray wavelength (the wavelength of $\text{CuK}\alpha$ radiation is 0.15418 nm), β is the full width at half maximum of the reflection, and θ is the diffraction angle.

In the final stage of our work, we used dynamic light scattering to determine the size and size distribution of the synthesized nanoparticles. Nanoparticle suspensions were prepared in *n*-hexane and their con-

centration was 1000 ppm. For each sample, results were obtained by averaging over three measurements performed in 90 s.

According to the DLS data in Fig. 7, the particle size distribution is centered at 86 nm for the copper nanoparticles, at 56 nm for the Cu@Cu₂O nanoparticles, and at 7 nm for the CuO nanoparticles. The large difference in particle size between the first two samples is due to the strong tendency for nanoparticles to agglomerate.

The present low-temperature (77 K) nitrogen adsorption results are presented in Table 1. The spherical shape of the synthesized nanoparticles (according

Table 1. Characteristics of the nanoparticles

Sample	S^{BET} , m ² /g	S^{STSA} , m ² /g	D^{BET} , nm	D^{TEM} , nm	D^{XRD} , nm	D^{DLS} , nm
Cu	17.2	17.3	39	36	37	86
Cu@Cu ₂ O	21.4	21.7	—	31	34	56
CuO	119.8	122.1	8	5	6	7

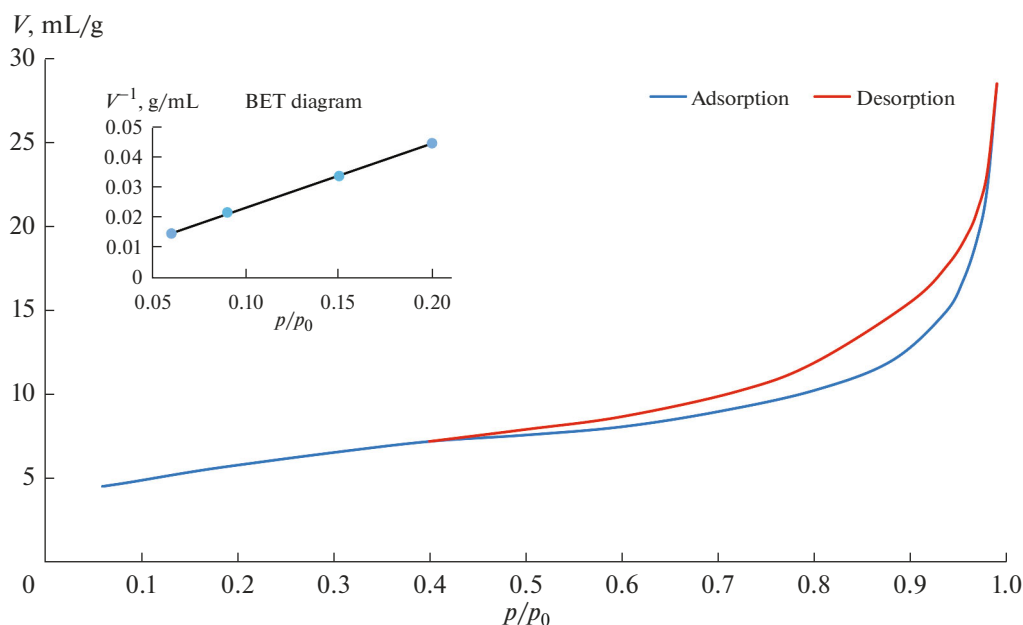


Fig. 8. Adsorption–desorption isotherm for the copper nanoparticles.

to TEM results) made it possible to estimate their average size from BET surface area data:

$$D_{\text{BET}} = \frac{6}{S_p}. \quad (2)$$

The nitrogen adsorption–desorption isotherms thus obtained for all three samples were similar in shape. Figure 8 shows the nitrogen adsorption–desorption isotherm for the copper nanoparticles. According to the IUPAC classification, this is a type IV isotherm, characteristic of mesoporous structures. Moreover, the observed hysteresis, due to capillary condensation, can be classified as the H3 type. This type of hysteresis is typical of solids containing slit pores due to agglomeration processes.

CONCLUSIONS

Cu, Cu@Cu₂O, and CuO nanoparticles have been prepared by the IFL method and shown to be less than 40 nm in size and have a crystal structure.

The absence of reflections from any impurity components in the X-ray diffraction patterns of all three samples suggests that the IFL method allows one to synthesize high-purity nanoparticles, which is due to contactless heating of the material, the single-step nature of the process, and the absence of additional reagents in the nanoparticles synthesis process.

We examined the feasibility of preparing nanoparticles differing in morphology by varying the amount of oxygen delivered to the reactor. Reducing the gas pressure in the apparatus ensured a sharp decrease in the average size of nanoparticles synthesized by the IFL method, down to a few nanometers. All of the

samples have been characterized by a variety of physicochemical methods.

IFL has been shown to be an environmentally friendly method. It can be used for synthesis of nanoparticles with controlled morphology in continuous mode at a high production rate.

FUNDING

This work was supported in part by the Russian Federation Ministry of Science and Higher Education (optimization of the operation of the experimental setup, research project no. FSWR-2022-0008) and Lobachevsky State University (physicochemical characterization of the materials, Priority 2030 Academic Leadership Program, project no. N-474-99, 2021–2023).

CONFLICT OF INTEREST

The authors declare that they have no conflicts of interest.

REFERENCES

1. Feynman, R., *Nanomaterials*, *Nanomaterials*, 2009, pp. 1–20.
2. Taylor, R., Coulombe, S., Otanicar, T., Phelan, P., Gunawan, A., Lv, W., Rosengarten, G., Prasher, R., and Tyagi, H., Small particles, big impacts: a review of the diverse applications of nanofluids, *J. Appl. Phys.*, 2013, vol. 113, no. 1, p. 011301.
3. Astruc, D., Introduction: nanoparticles in catalysis, *Chem. Rev.*, 2020, vol. 120, no. 2, pp. 461–463.
4. Malekzad, H., Sahandi Zangabad, P., Mirshekari, H., Karimi, M., and Hamblin, M., Noble metal nanoparti-

- cles in biosensors: recent studies and applications, *Nanotechnol. Rev.*, 2017, vol. 6, no. 3, pp. 301–329.
5. Liu, S., Fu, S., Zhang, X., Wang, X., Kang, L., Han, X., Chen, X., Wu, J., and Liu, Y., UV-resistant holographic data storage in noble-metal/semiconductor nanocomposite films with electron-acceptors, *Opt. Mater. Express*, 2018, vol. 8, no. 5, pp. 1143–1153.
 6. Taylor, R., Phelan, P., Otanicar, T., Adrian, R., and Prasher, R., Nanofluid optical property characterization: towards efficient direct absorption solar collectors, *Nanoscale Res. Lett.*, 2011, vol. 6, no. 1, pp. 1–11.
 7. Abass, S.M., Sunitha, S., Ashaq, S.M., Khadheer, P.S., and Choi, D., An overview of antimicrobial and anticancer potential of silver nanoparticles, *J. King Saud Univ., Sci.*, 2022, vol. 34, no. 2, p. 101791.
 8. Ullah, K.A., Chen, L., and Ge, G., Recent development for biomedical applications of magnetic nanoparticles, *Inorg. Chem. Commun.*, 2021, vol. 134, p. 108995.
 9. Shahbazali, E., Hessel, V., Noël, T., and Wang, Q., Metallic nanoparticles made in flow and their catalytic applications in organic synthesis, *Nanotechnol. Rev.*, 2014, vol. 3, no. 1, pp. 65–86.
 10. Ojha, N., Zyryanov, G., Majee, A., Charushin, V., Chupakhin, O., and Santra, S., Copper nanoparticles as inexpensive and efficient catalyst: a valuable contribution in organic synthesis, *Coord. Chem. Rev.*, 2017, vol. 353, pp. 1–57.
 11. Fathima, J., Pugazhendhi, A., Oves, M., and Venis, R., Synthesis of eco-friendly copper nanoparticles for augmentation of catalytic degradation of organic dyes, *J. Mol. Liq.*, 2018, vol. 260, pp. 1–8.
 12. Kang, J., Kim, H., Ryu, J., Thomas, H.H., Jang, S., and Joung, J., Inkjet printed electronics using copper nanoparticle ink, *J. Mater. Sci. Mater. Electron.*, 2010, vol. 21, no. 11, pp. 1213–1220.
 13. Kubota, S., Morioka, T., Takesue, M., Hayashi, H., Watanabe, M., and Smith, R., Continuous supercritical hydrothermal synthesis of dispersible zero-valent copper nanoparticles for ink applications in printed electronics, *J. Supercrit. Fluids*, 2014, vol. 86, pp. 33–40.
 14. Kruk, T., Szczepanowicz, K., Stefanska, J., Socha, R., and Warszynski, P., Synthesis and antimicrobial activity of monodisperse copper nanoparticles, *Colloids Surf. B*, 2015, vol. 128, pp. 17–22.
 15. Rajeshkumar, S., Menon, S., Venkat, K.S., Tambuwala, M., Bakshi, H., Mehta, M., Satija, S., Gupta, G., Chellappan, D., Thangavelu, L., and Dua, K., Antibacterial and antioxidant potential of biosynthesized copper nanoparticles mediated through *Cissus arnotiana* plant extract, *J. Photochem. Photobiol.*, 2019, vol. 197, p. 111531.
 16. Calabrese, C., La, P.V., Testa, M., and Liotta, L., Antifouling and antimicrobial activity of Ag, Cu and Fe nanoparticles supported on silica and titania, *Inorg. Chim. Acta*, 2022, vol. 529, p. 120636.
 17. Yabuki, A. and Tanaka, S., Oxidation behavior of copper nanoparticles at low temperature, *Mater. Res. Bull.*, 2011, vol. 46, no. 12, pp. 2323–2327.
 18. Kim, I., Kim, Y., Woo, K., Ryu, E., Yon, K., Cao, G., and Moon, J., Synthesis of oxidation-resistant core-shell copper nanoparticles, *RSC Adv.*, 2013, vol. 3, no. 35, pp. 15169–15177.
 19. Wang, H., Cheng, S., Cai, X., Cheng, L., Zhou, R., Hou, T., and Li, Y., Photocatalytic CO₂ reduction to HCOOH over core-shell Cu@Cu₂O catalysts, *Catal. Commun.*, 2022, vol. 162, p. 106372.
 20. Kalidindi, S.B., Sanyal, U., and Jagirdar, B.R., Nanostructured Cu and Cu@Cu₂O core shell catalysts for hydrogen generation from ammonia-borane, *Phys. Chem. Chem. Phys.*, 2008, vol. 10, no. 38, pp. 5870–5874.
 21. Mayyas, A., Wei, M., and Levis, G., Hydrogen as a long-term, large-scale energy storage solution when coupled with renewable energy sources or grids with dynamic electricity pricing schemes, *Int. J. Hydrogen Energy*, 2020, vol. 45, no. 33, pp. 16311–16325.
 22. Sadrolhosseini, A., Noor, A., Shameli, K., Mamdoohi, G., Moksini, M., and Adzir, M.M., Laser ablation synthesis and optical properties of copper nanoparticles, *J. Mater. Res.*, 2013, vol. 28, no. 18, pp. 2629–2636.
 23. Khayati, G., Nourafkan, E., Karimi, G., and Moradgholi, J., Synthesis of cuprous oxide nanoparticles by mechanochemical oxidation of copper in high planetary energy ball mill, *Adv. Powder Technol.*, 2013, vol. 24, no. 1, pp. 301–305.
 24. Richter, K., Birkner, A., and Mudring, A., Stabilizer-free metal nanoparticles and metal-metal oxide nanocomposites with long-term stability prepared by physical vapor deposition into ionic liquids, *Angew. Chem., Int. Ed.*, 2010, vol. 49, no. 13, pp. 2431–2435.
 25. Jia, F., Zhang, L., Shang, X., and Yang, Y., Non-aqueous sol-gel approach towards the controllable synthesis of nickel nanospheres, nanowires, and nanoflowers, *Adv. Mater.*, 2008, vol. 20, no. 5, pp. 1050–1054.
 26. Zhang, Q., Yang, Z., Ding, B., Lan, X., and Guo, Y., Preparation of copper nanoparticles by chemical reduction method using potassium borohydride, *Trans. Nonferrous Met. Soc. China*, 2010, vol. 20, suppl. 1, pp. s240–s244.
 27. Vijay, K.R., Elgamiel, R., Diamant, Y., Gedanken, A., and Norwig, J., Sonochemical preparation and characterization of nanocrystalline copper oxide embedded in poly(vinyl alcohol) and its effect on crystal growth of copper oxide, *Langmuir*, 2001, vol. 17, no. 5, pp. 1406–1410.
 28. Huang, L., Jiang, H., Zhang, J., Zhang, Z., and Zhang, P., Synthesis of copper nanoparticles containing diamond-like carbon films by electrochemical method, *Electrochem. Commun.*, 2006, vol. 8, no. 2, pp. 262–266.
 29. Markov, A.N., Vorotyntsev, A.V., and Andronova, A.A., Direct synthesis of titanium nanoparticles by induction flow levitation technique, *Key Eng. Mater.*, 2021, vol. 887, pp. 178–183.
 30. Kuskov, M., Zhigach, A., Leipunsky, I., Afanasenkova, E., Safronova, O., Berezkina, N., and Vorobjeva, G., Synthesis of nanopowders of titanium compounds via flow-levitation method and study their properties, *IOP Conf. Ser. Mater. Sci. Eng.*, 2019, vol. 558, no. 1, p. 012023.

Translated by O. Tsarev